Corresponding author: Tel.: +47 735 937 48; fax: + 47 735 953 10.

# DEVELOPMENT OF ONE-DIMENSIONAL MODEL FOR INITIAL DESIGN AND EVALUATION OF OIL-FREE $CO_2$ TURBO-COMPRESSOR

**Bartosz Kus(a) and Petter Nekså(b)**

(a) Norwegian University of Science and Technology

7491 Trondheim, Norway

Bartosz.Kus@ntnu.no

(b) Norwegian University of Science and Technology

7491 Trondheim, Norway

Petter.Neksa@sintef.no

## ABSTRACT

A 1-dimenional tool for preliminary design and performance prediction of oil-free $CO_2$ compressor is presented. The model describes high speed centrifugal compressor in a hermetic configuration supported on foil gas bearings. To give possibly comprehensive overview of the technology, a wide range of loss mechanisms is considered. The model predicts aerodynamic performance of the compressor as well as losses related to the windage of rotor and bearings and due to the internal cooling. Numerical investigation of different compressor stages was used to validate aerodynamic predictions of the 1D model. Maximal prediction discrepancy amounted 2% for efficiency and 5% for pressure ratio. The prediction of the total compressor efficiency was compared with test data from a 50kW compressor published Sandia Laboratories. The predicted peak compressor efficiencies are between 66-67.5% while experimentally measured values are within 65-70% region.

## KEYWORDS

Radial turbo-compressor, $CO_2$ compression, Oil-free compressors, Oil-free refrigeration

## 1. INTRODUCTION

Popularity of carbon dioxide as a working medium has been gaining momentum in the last decade. It is motivated not only by increased environmental awareness of the society but economical factor as well. $CO_2$ installations can be more compact than its hydrocarbon- or synthetic- counterparts and in many cases more energy efficient [Nekså et.al. (2010), "NARECO2" (2009), Chen et. al. (2006)]. Recent development in supercritical $CO_2$ power cycles has brought attention to the new type of machines used in the $CO_2$ field, namely high speed oil-free turbo-compressors and turbo-expanders. Sandia National Laboratories (SNL) has published a report [(Wright et. al. (2010)] from successful testing of 50 kW radial compressor spinning at up to 75 krpm and producing pressure ratios of up to 1.8. Although rather low efficiencies of the compressor are reported, such a concept can be perceived as an interesting option for other $CO_2$ based systems, such as air conditioning or refrigeration. Benefits of oil-free operation are multiple and include simplified architecture of the system, broader range of operating conditions [Hafner et. al. (2011)] and improved heat exchange.

Schiffmann and Favrat (2009, 2010) have designed and successfully tested small oil-free radial compressor for domestic heat pump utilizing R134a as a working fluid. 78% isentropic efficiency is reported for a small 20 mm impeller reaching pressure ratios in excess of 3.3. Mechanical efficiency quantifying windage losses is calculated to be in the range of 92-95%. It is expected that such a high mechanical efficiency will be very difficult to reach for $CO_2$ systems due to the significantly higher density of the gas.

To gain more understanding about which applications and what operating conditions are particularly interesting for the new type of machine, efficient design tools must be available. The purpose of the present study is to introduce a tool that allows for quick prediction of basic dimensions and performance of $CO_2$ oil-free compressor based on a set of designer inputs.

The importance of reliable preliminary estimation of compressor parameters should not be underestimated as an early identification of performance potential can save a lot of time and resources in subsequent phases of the system development as well as in its operation. It is expected that the tool could be used as a very first step in the machine design, providing rapid identification of possibly weak points of the technology depending on a particular field of application.

The 1D model consists of two essential parts. The first part predicts aerodynamic performance of a centrifugal compressor stage. The second one models losses resulting from hermetic operation and includes gas bearing friction, rotor windage and internal cooling losses.

One- or two-stage configuration can be simulated. The preliminary validation of the tool is based on CFD analysis and test data presented in the SNL report [(Wright et. al. (2010)]. Configuration of the two-stage compressor with brushless permanent magnet motor is shown in Fig 1.

The presented model is used in Kus and Nekså (2013), where more comprehensive overview of the oil-free $CO_2$ compression technology is given, to assess feasibility of introducing oil-free turbo-compressors into commercial and industrial $CO_2$ refrigeration applications.

## 2. MODELLING

### 2.1 Tool structure

The design tool has been made with a Microsoft Excel interface where a user has the full control of all important model constants and assumptions. These involve: impeller clearance, axial length of impeller (as a fraction of impeller diameter), inducer diameter ratio, diffuser diameter ratio, mean inducer blade angle, impeller discharge flow angle, magnetic shear stress of the motor, thrust bearing diameter ratio, motor electric efficiency, labyrinth seal dimensions, radial gap in journal bearings, load capacity of the gas bearings and internal cooling ratio (degree of cooling that is performed by fraction of the compressed gas).

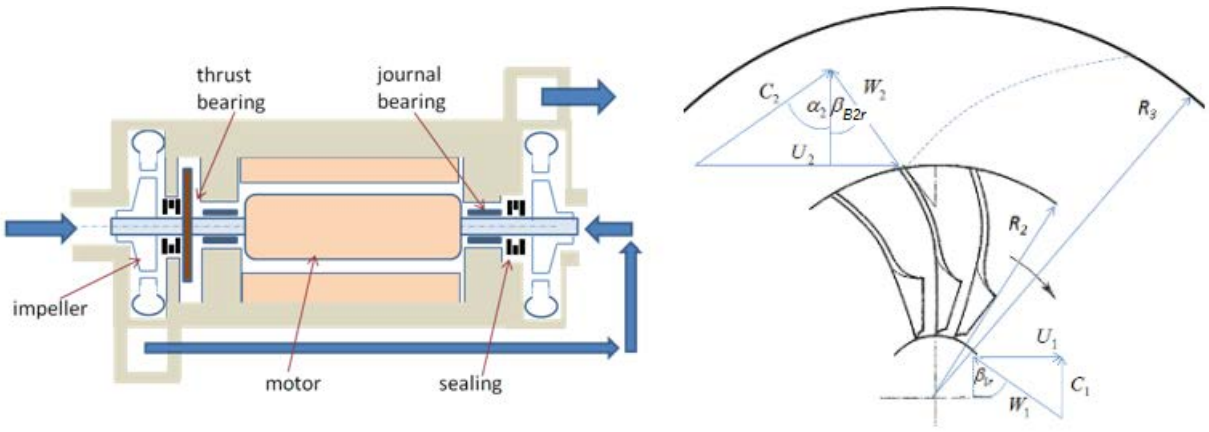


Figure 1. 2-stage compressor configuration

The procedure itself takes place in VBA macros activated from the interface sheet. The algorithm contains three main iteration loops; the first two calculating dimensions and aerodynamic performance of the stages and the third one calculating the total machine's performance including additional losses generated by windage, electrical components and the cooling flow (see Fig 2). The tool also predicts basic dimensions of bearings, rotor and shaft.

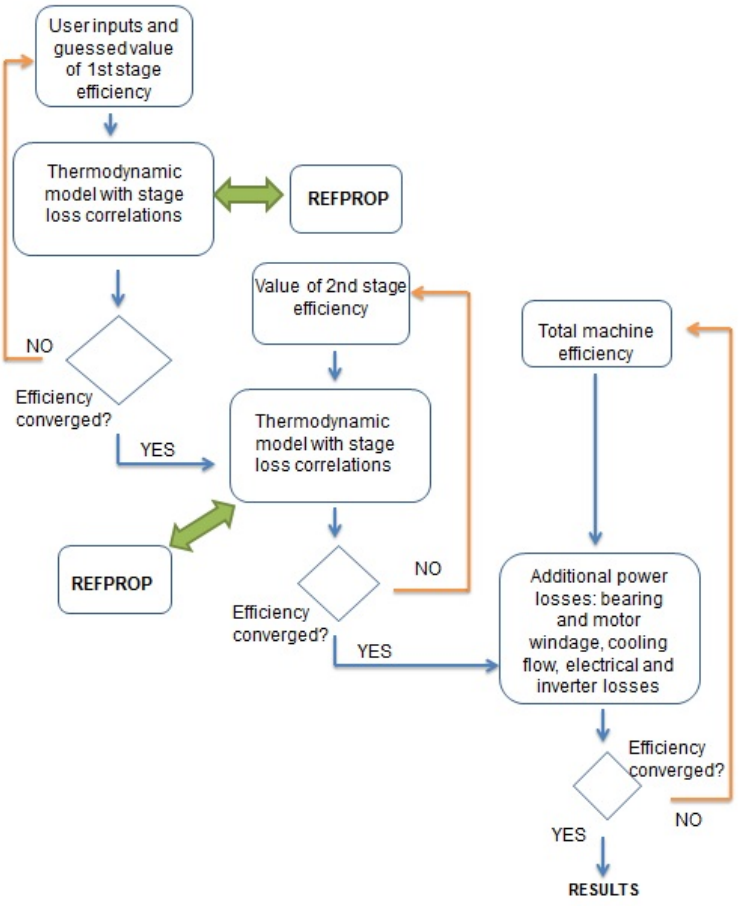


Figure 2. The calculation tool structure under Refprop thermodynamic data library

**2.2 Aerodynamic modeling**

It was decided to base the design procedure on 1D (mean line) approach, treating a compressor stage as a set of characteristic parts, each defined by inlet and outlet surfaces. Losses occurring in each of these parts are modeled with empirical correlations developed during the past several decades. The mean line method is regarded as a most practical one and providing acceptable accuracy [Oh et. al. (1997), Sungho and Baek (2001)]. Furthermore, a tool based on basic

thermodynamic equations and pointing out specific loss mechanisms has also significant educational valor. It gives a designer an opportunity to test impact of particular design choices on the final performance of the machine.

Table 1 presents loss models used in the present study.

Table 1. Loss correlations

| Loss mechanism | Loss model | Reference |
|---|---|---|
| **Blade loading loss:** occurs due to the boundary layer growth, separation and secondary flow development | $\Delta h_{bl} = 0.05 D_f{}^2 U_2^2$<br>$D_f = 1 - \frac{W_2}{W_{1t}} + \frac{0.75 \Delta h_{Euler} / U_2^2}{(W_{1s}/W_2)\left[(Z/\pi)(1 - D_{1t}/D_2) + 2D_{1t}/D_2\right]}$<br>$\Delta h_{Euler} = C_{\theta 2} U_2 - C_{\theta 1} U_1$ | Coppage et. al. (1956) |
| **Impeller skin friction:** is generated by the viscous shear forces in the flow boundary layers. The procedure is equivalent to the pipe flow friction calculation | $\Delta h_{sf} = 2 c_{fi} (L_i / D_{ih}) W_m^2$<br>$W_m = \frac{C_{1t} + C_2 + W_{1t} + 2W_{1h} + 3W_2}{8}$<br>$c_{fi} = 0.3164 (\mathrm{Re}_i)^{-0.25}$ | Jansen (1967) |
| **Vaneless diffuser loss:** The procedure is similar to impeller loss calculation, but the velocity is assumed to be the mean value of inlet and outlet diffuser velocities | $\Delta h_{df} = 2 c_{fd} (L_d / D_{dh}) C_m^2$<br>$c_{fd} = k \left( \frac{1.8 \cdot 10^5}{\mathrm{Re}_d} \right)^{0.2}$<br>$k = 0.015$ | Japikse (1982) |
| **Clearance loss:** results from the leakage of the fluid from the pressure to the suction side of the unshrouded impeller blades | $\Delta h_{cl} = 0.6 \frac{\varepsilon}{b_2} C_{\theta 2} \left\{ \frac{4\pi}{b_2 Z_b} \left[ \frac{r_{1s}^2 - r_{1h}^2}{(r_2 - r_{1t})(1 + \rho_2/\rho_1)} \right] C_{\theta 2} C_{r1} \right\}$ | Jansen (1967) |

| | | |
|---|---|---|
| **Mixing loss:** is a result of non-uniform discharge of the flow from the impeller and is calculated based on the jet/wake theory | $\Delta h_{mix} = \frac{1}{1+\tan^2 \alpha_{2r}} \left( \frac{1-\varepsilon_{wake}-b^*}{1-\varepsilon_{wake}} \right)^2 \frac{C_2^2}{2}$<br>where: $\varepsilon_{wake}$ =0.25, b*=1 | Johnston and Dean (1966)<br>Oh et. al. (1997) |
| **Disc friction loss:** Is generated by the shear flow forces acting on the impeller backplate | $\Delta h_{disc} = C_{f\,disc} \frac{\overline{\rho} r_2^2 U_2^3}{4\dot{m}}$<br>$\begin{cases} \frac{2.67}{\mathrm{Re}_{disc}^{0.5}}, & \mathrm{Re}_{disc} < 3x10^5 \\ \frac{0.0622}{\mathrm{Re}_{disc}^{0.2}}, & \mathrm{Re}_{disc} > 3x10^5 \end{cases}$<br>$\mathrm{Re}_{disc} = \frac{U_2 r_2}{\nu_2} \qquad \overline{\rho} = \frac{\rho_1 + \rho_2}{2}$ | Daily and Nece (1960) |
| **Recirculation loss:** results from reversal into the impeller of a portion of the flow that does not have enough momentum to overcome pressure gradients in the diffuser | $\Delta h_{rc} = 0.02 D_f^2 U_2^2 \sqrt{\tan \alpha_{2r}}$ | Jansen (1967) |
| **Volute loss:** It is assumed that the meridional velocity component of the fluid leaving the diffuser is lost in the volute | $\Delta h_{vol} = C_{3r}^2 / 2$ | |

The basic design procedure is given below.

**1D design procedure**

The specific work needed to compress the fluid to required pressure is calculated according to:

$$W_{comp} = \left(h_{02s} - h_{00}\right)\eta_{s\,total} \tag{1}$$

where both enthalpies are calculated by the REFPROP code based on the designer inputs: the inlet temperature and pressure and discharge pressure. The total isentropic efficiency is assumed to start first main iteration loop.

Total discharge conditions are calculated from the isentropic efficiency definition:

$$\eta_{s\,total} = \frac{\left(h_{02s} - h_{00}\right)}{\left(h_{02} - h_{00}\right)} \tag{2}$$

An inlet velocity triangle is established in an iterative procedure so as to satisfy the requirement of the assumed inlet relative flow angle $\beta_{1\,r}$ (mean) and $D_{1h}/D_{1t}$ ratio. The admission of the gas at the impeller inlet is axial.

The discharge velocity triangle is established from Euler equation:

$$\frac{P_{comp}}{\dot{m}} = U_2 C_{\theta 2} \tag{3}$$

and includes reduction of tangential velocity component by backward blade sweep $\beta_{B2}$ and slip $\sigma$, according to equations:

$$C_{\theta 2} = \sigma U_2 + C_r \tan\beta_{B2} \tag{4}$$

$$\sigma = 1 - \frac{0.63\pi}{Z_B} \tag{5}$$

The above procedure aims at providing specified impeller discharge absolute flow angle $\alpha_{2r}$.

With calculated discharge blade tip speed $U_2$ and assumed rotational speed one can easily find impeller discharge diameter:

$$D_2 = \frac{U_2}{\pi\omega} \tag{6}$$

To calculate impeller discharge blade height $b_2$ discharge static gas conditions have to be known. These are found from calculated (based on loss corellations) impeller efficiency. Determination of vaneless diffuser ideal discharge velocity triangle is based on two equations known as mass conservation equation and angular momentum equation.

$$\dot{m} = \rho_2 A_2 C_{r2} = \rho_3 A_3 C_{r3} \tag{7}$$

$$\tau = \dot{m}\left(r_3 C_{\theta 3} - r_2 C_{\theta 2}\right) \tag{8}$$

Real diffuser discharge conditions are calculated based on the total compressor discharge temperature and calculated passage losses.

Once the main stage dimensions and properties of the gas in the characteristic sections of the compressor are established, the loss correlations can be employed to predict the stage efficiency.

$$\eta_{s\,total} = \frac{\left(h_{02s} - h_{00}\right)}{\left(h_{02} - h_{00}\right)} = \frac{\left(h_{02s} - h_{00}\right)}{\left(h_{02s} - h_{00}\right) + \sum \Delta h_{loss}} \tag{9}$$

Calculated efficiency is then compared with the initially provided value and the iteration loop will be repeated until both values match within the tolerance specified by the user. Analogical procedure is applied to predict efficiency of the second stage and the overall compressor efficiency.

After convergence of the calculation some general performance coefficients can be defined and calculated to judge the design of the compressor stage. These may include:

**Flow rate coefficient**

$$\phi = \frac{Q}{U_2 d_2^2} \frac{4}{\pi} \tag{10}$$

**Work coefficient**

$$\psi = \frac{\Delta h_{t-t}}{U_2^2} \tag{11}$$

**Machine Mach Number**

$$M_U = \frac{U_2}{a_{01}} \tag{12}$$

**Machine Reynolds Number**

$$\mathrm{Re} = \frac{U_2 D_2}{\upsilon_{01}} \tag{13}$$

**Specific speed**

$$N_s = \frac{\omega\sqrt{Q}}{\Delta h_{0s}^{0.75}} \tag{14}$$

### 2.3 Rotor windage modeling

It is identified that high speed motors operating in high ambient pressure tend to induce windage losses that cannot be neglected in the initial design of the compressor [Briggs et. al. (2008), Wright et al. (2010)].

While there are many correlations well proven for some specific operating conditions [Raymond et. al. (2008), Walton et. al. (2012)] present study will use correlation (1) developed by Vrancik (1968) and validated for high speed $CO_2$ compressor [Wright et. al. (2010)].

$$P_{mw} = \pi C_f \rho R^4 \omega^3 L \tag{15}$$

*where:*

$$\frac{1}{\sqrt{C_f}} = 2.04 + 1.768 \ln( \mathrm{Re} \sqrt{C_f} ) \tag{16}$$

Dimensions of the rotor are determined from the formula found in Hanselman (2006):

$$TRV = \frac{\tau}{\frac{\pi}{4} D_{mot}^2 L_{mot}} \tag{17}$$

*where:*

$$TRV = 2\sigma_m \tag{18}$$

Required torque is calculated from compressor power and angular speed. Important design parameter is the gap sheer stress which is the tangential force per unit rotor surface area. When expressed in Pa units, low cost brushless permanent magnet motors typically exhibit a shear stress in the range of $3400<\sigma_m<13800$ ($0.5<\sigma_m<2$ psi), higher cost motors in the range $10300< \sigma_m <20600$ ($1.5< \sigma_m <3$ psi), very high performance motors are typically in the range $13800< \sigma_m <69000$ ($2< \sigma_m <10$ psi), and large liquid cooled motors $69000< \sigma_m <138000$ ($10< \sigma_m <20$ psi). The designer must also decide on L/D ratio of the rotor. To reduce windage losses it is desirable to have long slender rotor. One have to bear in mind however that longer motors are more likely to exhibit rotordynamics issues, especially pronounced in machines with gas foil bearings. For Sandia's $CO_2$ compressor L/D ratio amounted to 3.7 [Wright et. al. (2010)]. Final size of the motor should always be preceded by rotordynamics analysis.

Rotor tip speed must be also checked. The limiting constraint is to keep the magnets in compression. Depending on the magnets material different peripheral speeds can be allowed. For a high strength, low resistivity and high modulus material such as Inconel 718 maximum rotor peripheral speed of 200 m s-1 is acceptable.

**2.4 Gas bearings modeling**

Estimation of gas bearing losses consists of three stages: predicting radial and axial forces acting on the rotor, sizing the bearing based on bearing load capacities and applying an appropriate loss model.

**Predicting axial loads**

Simple 1D prediction of axial loads in a $CO_2$ centrifugal compressor is a subject to a significant uncertainty. There can be up to few tens of thousands N of force across the front and back face of the impeller, therefore the model must subtract two very large numbers. It means that not only prediction of thrust magnitude but also its direction could be challenging. Noall and Batton (2011) used a 1D correlation to predict thrust in a radial turbine working in supercritical state for $CO_2$. Measurements showed that actual thrust was not only a third of the predicted one, but also acted in the opposite direction. It is more difficult to predict static pressures at a radial turbine's intermediate stations than in radial compressors; however it shows that simple mathematical operations with big numbers can give misleading results.

During testing of the $SCO_2$ (supercritical $CO_2$) compressor performed by SNL [(Wright et. al. (2010)] the following approach was taken. First, the rotor was installed on typical roller bearings and during the initial tests a load cell was used to measure the thrust. The compressor was equipped with pump out vanes on the back side of the impeller wheel. Gradual trimming of the vane outer radius allowed for balancing of the axial loads. Once the load cell indicated magnitudes of thrust acceptable for gas bearings they were installed instead of ball bearings.

The literature suggests that CFD methods can be reliable sources of information about axial forces acting on centrifugal compressor impeller. Shi et. al. (2010) used numerical simulations to predict axial thrust in a deep well pump. Comparison of simulation results with measured values gave error of 0.3-5.9 % across the full range of operating conditions.

An attempt to validate the CFD model against experimental data published by Sandia is made in the present study. 3D model (Fig 3) of compressor stage was generated based on the geometrical description provided in the SNL report. Numerical simulation was conducted with FLUENT 13 code. The turbulence was predicted with the k-ε model and wall boundary layers were solved with wall functions. The second-order discretization scheme was used for simulations. Inlet conditions of the tested compressor were very close to the critical point. It resulted in simulation convergence problem when real gas (REFPROP) equations were used to determine thermodynamic properties of gas. Changing inlet boundary conditions to higher temperature and higher pressure would solve convergence issues as the solver would have more "space" to search for a solution around the assigned boundary conditions without crossing the saturation line. Simulating the compressor with different pressure levels does not however enable direct validation of

CFD method against the experimental data. The approach taken was instead to use constant density model and reach simulation convergence maintaining inlet boundary conditions in accordance with test data. Sandia actually used the test data to adjust their 1D model for thrust prediction based on incompressible gas equations. Good agreement was achieved.

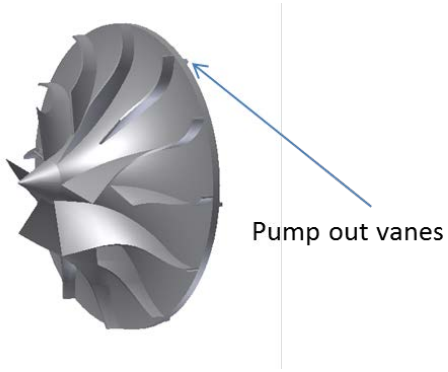


Figure 3. 3D model of Sandia's impeller with pump out vanes

**CFD simulation of Sandia's compressor**

Simulation parameters are presented in Table 2

Table 2

| **Parameter** | Inlet mass flow, kg s-1 | Inlet static pressure, bar | Outlet static pressure, bar | Density, kg m-3 | Rotational speed, rpm | Pump out vane clearance, mm |
|---|---|---|---|---|---|---|
| **Value** | 3.96 | 80 | 93.85 | 630 | 40 000 | 0.15 |

To reduce computational effort periodic boundary condition was applied and only 1/6 of the compressor domain was used for simulation.

Figure 4 presents predicted thrust load acting on the full impeller versus grid size of the simulated domain. It is important to note that that presented results take into account thrust component resulting from cavity pressure acting on the compressor shaft. Shaft diameter and cavity pressure used for calculation are also taken from Sandia's report. It can be observed that direction of the thrust and its magnitude matches quite well with the data presented by Sandia, around 533 N (120 lbs) of force for 40k revolutions per minute. The not exact match can be attributed to the usage of the

constant density model instead of real gas equations and the not perfect reproduction of real compressor's blade curvature. The analysis however confirms that CFD can be a reliable tool for prediction of magnitude and direction of axial thrust acting in a centrifugal compressor.

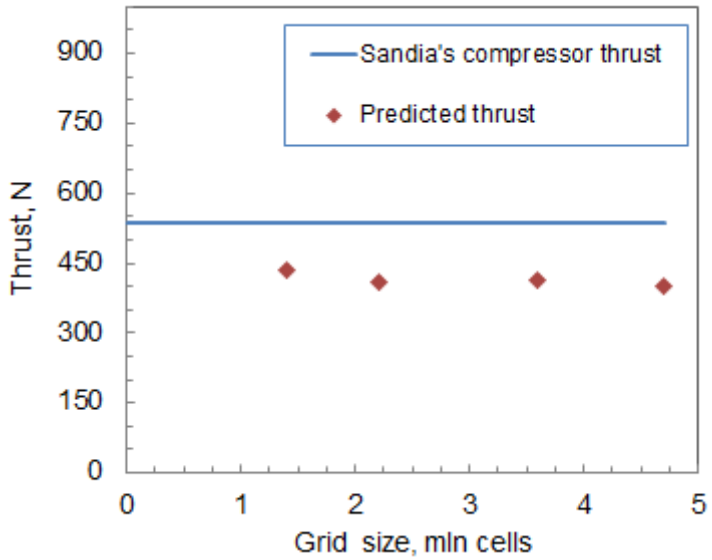


Figure 4. Mesh independence study for prediction of axial thrust

Additional simulations were performed for 3 different impellers in order to get more insight into what magnitude of axial forces can be expected in $CO_2$ turbo-compressor. Parameters of each simulated stage are presented in more detail in the *Results* section of present paper. Predicted axial thrusts are shown in Fig 5. Negative values mean that resultant thrust acted towards compressor inlet, positive ones indicate thrust direction towards impeller back plate.

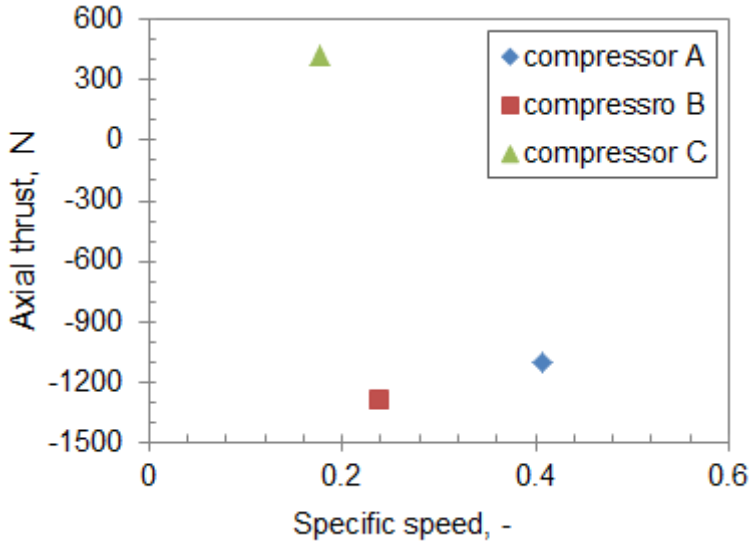


Figure 5. Prediction of axial thrust for different $CO_2$ compressors

It is shown that axial forces acting in $CO_2$ turbo-compressors can be of significant value and due to the complex 3-dimentional nature of the gas flow it is difficult to predict them in a quick analytical way. There seems to be a potential however to use CFD results as an input for development of more accurate 1D models in the future. So far, if a quick performance prediction of oil-free $CO_2$ compressor is needed, the magnitude of thrust should be assumed on some reasonable level, to provide for its future balancing with assistance of CFD or experimental methods.

**Sizing a thrust bearing**

Widely accepted "rule-of-thumb" for load capacity (expressed in N) that can be supported by a thrust foil bearing is given by (5):

$$W_{LC\,AB} = f_{AB}(\pi \mathrm{w} D_{AB\,m}) D_{AB\,m} N \tag{19}$$

where:

w - difference between the inner and outer top foil diameters or radial extent of the top foil (m);

N – shaft speed (krpm)

Dykas et al. (2009) cites different load coefficients obtained by various researchers. They vary from 664 to 3460 kg m-3 Krpm-1 (0.024 to 0.125 lb in-3 Krpm-1) for different rotational speeds. New generation of bearings is reported to achieve load coefficients of around 2770 kg m-3 Krpm-1 (0.1 lb in-3 Krpm-1) and this value is proposed to be used with the present model. The above equation can be used to calculate the size of axial bearing once the axial load is determined.

**Windage of thrust bearing**

Calculation of the power loss generated by the thrust bearing employs the theory of flow around a disc rotating in a housing and is presented in Schlichting (1968). It defines a dimensionless torque coefficient $c_M$ from the laminar "free" rotating disc case (6).

$$c_M = \frac{\tau}{0.5 \rho_{cav} \omega^2 r^5} \tag{20}$$

Correlations for turbulent torque coefficient were proposed by various authors.

Recent windage measurements of foil bearing rotating in supercritical state $CO_2$ was presented by Milone (2010). It shows significant underestimation of the torque coefficient by the often used Schultz-Grunow formula (see Fig 7). The overview of other correlations developed for free rotating disc case is presented in Miles (2011). It is found that correlations given by von Kármán (1921), Dorfman (1958) and Bayley and Owen (1969) match quite well with test data obtained for free rotating disc in pressurized air. Superimposing all three correlations to supercritical $CO_2$ conditions also gives a reasonable match (Fig 6). The Bayley and Owen formula will be used as a default setting in the present tool.

| | | |
|---|---|---|
| Schultz-Grunow | $c_M = 0.0622(\mathrm{Re})^{-1/5}$ | (21) |
| von Kármán | $c_M = 0.146(\mathrm{Re})^{-0.2}$ | (22) |
| Dorfman | $c_M = 0.982(\log_{10}\mathrm{Re})^{-2.58}$ | (23) |
| Bayley and Owen | $c_M = 0.131(\mathrm{Re})^{-0.186}$ | (24) |
| | where: $\mathrm{Re} = \frac{r^2\omega}{\upsilon}$ | (25) |

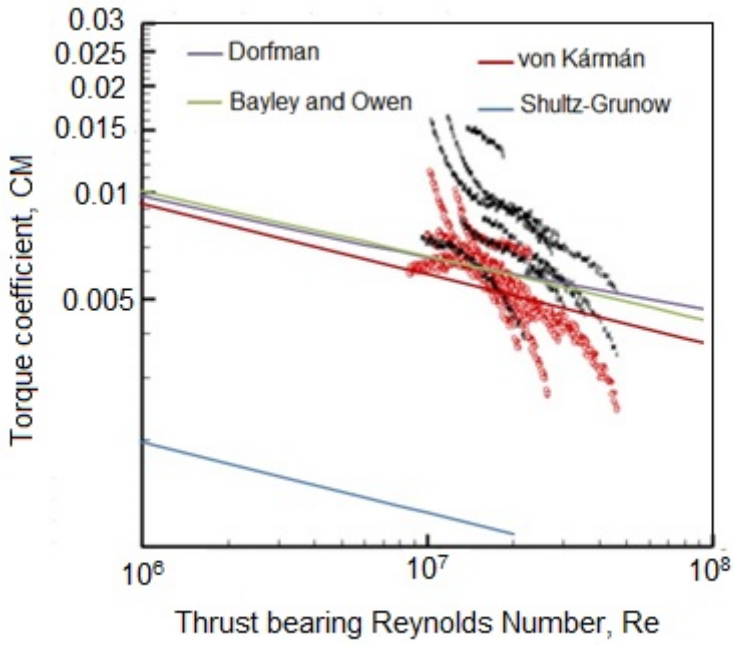


Figure 6. Theoretical torque coefficients for free rotating disc versus experimental data for supercritical $CO_2$ conditions

Once the torque coefficient is estimated the power loss of the thrust bearing can be calculated:

$$P_{AB} = 0.5 c_M \rho \omega^3 \left( r_0^5 - r_{in}^5 \right) \tag{26}$$

**Radial load prediction**

Provided rotor dimensions and its construction material density, one can simply calculate the radial force that is generated on the journal bearings. Radial force resulting from non-uniform pressure distribution across the volute of the compressor is believed to be negligible in the design point operation and thus is not taken into account [Reunanen and Larjola (2005)].

**Sizing a radial bearing**

Load capacity that can be supported by a journal bearing is given by:

$$W_{LC\,JB} = f_{JB}(L_{JB} D_{JB}) D_{JB} N \tag{27}$$

Typical advanced journal foil bearing performance coefficient value $f_{JB}$ expressed in kg m-3 krpm-1 is 27680 (1 lb in-3 krpm-1) [Dykas et al. (2009)]. If calculated dimensions are smaller than the journal foil bearings commercially available on the market, they are scaled up to match commercial bearings sizes. Minimum diameter of a journal bearing is assumed to be 30 mm.

**Windage of radial bearing**

It is proposed that foil journal bearing can be treated as a special case of rotor-stator system where the outer cylinder is at rest and the inner is rotating and modeled with Taylor-Couette flow theory [Schlichting (1968)]. The theory predicts three operational regimes which can be described by relating two non-dimensional numbers, the torque coefficient ($C_M$) and the Taylor number ($T_a$).

$$T_a = \frac{U_i \varepsilon}{\upsilon} \sqrt{\frac{\varepsilon}{r_i}} \tag{28}$$

$$C_M = \frac{Mi}{0.5 \pi \rho U_i^2 r_i^2 \varepsilon} \tag{29}$$

For Taylor numbers higher than 400 the flow becomes turbulent and this is the region where high speed bearings are expected to operate. The validation of the theory for high pressure and high speed $CO_2$ applications can be found in

Bruckner (2009) and Howard et.al. (2007). The measured toque coefficients obtained for various $CO_2$ pressures and rotor shafts fit reasonably well with the theoretical predictions.

To calculate windage of a journal bearing the following formula for turbulent torque coefficient can be used [Sukhomlinov et. al. (2003)]:

$$C_M = 0.02 T_a^{-0.2} \tag{30}$$

Power loss is then simply found from angular speed and torque relationship.

**2.5 Cooling loss modeling**

Hermetic $CO_2$ compressors require efficient cooling. It is known that friction losses occurring due to the rotor and bearing windage can be significant. Proven practice is to allow some ratio of the compressed gas to leak into the rotor cavity. Throttling of the gas in the clearance of the shaft seal will provide necessary cooling capacity needed to remove friction heat from bearings and the rotor. If labyrinth seals are used the actual mass flow of the cooling stream can be approximated by the "Martin" (17) formula and depends on the geometry of the seal, density of the gas and pressure levels on both sides of the seal.

$$m_l = C_d S_0 \sqrt{p1\rho1 \left( \frac{\left(1 - \frac{p_2}{p_1}\right)^2}{N - \ln\left(\frac{p_2}{p_1}\right)} \right)} \tag{31}$$

where: $S_0$ is the leakage area and $C_d$ is dimensionless discharge coefficient

The correlation was found to predict leakage reasonably well for a tested supercritical $CO_2$ compressor [Wright et. al. (2010)].

If assumed dimensions of the seal (diameter, number and height of the teeth) results in mass flows and cooling capacity not sufficient to remove friction losses then the geometry is changed iteratively to allow more coolant flow into the cavity.

The tool's default pressure value in the cavity is set to inlet pressure of the compressor. This eliminates the need for booster pump/compressor that would otherwise have to pump the leaked stream back into the compressor inlet pressure. The designer can however specify different pressure levels.

It is assumed that the heat removal process is isobaric. To find the mass flow required for cooling the cavity discharge temperature must be also provided. It is assumed to keep this temperature around 100 °C in order to keep the motor cool enough to perform efficient and safe operation.

The cooling loss is defined as a power needed to compress the stream leaving the cavity to the discharge pressure of the compressor. Efficiency of this process is assumed to be that of the compressor. Cooling demand generated by the windings of the electrical motor is not taken into account here. It is assumed that additional casing cooling will be provided.

## 3. RESULTS

### 3.1 CFD verification of stage performance

It is believed that CFD can be used as a reliable method to predict turbo-machinery internal flows. This was validated experimentally by Krain and Hah (2003), Roberts and Steed (2004), Swain (2005), Xu and Amano (2009). Therefore, an attempt to verify predictions of the 1D tool with CFD analysis was made.

Three different compressor geometries (Fig 7) were created based on the output from the 1D tool. Parameters for each compressor stage are collected in Table 3.

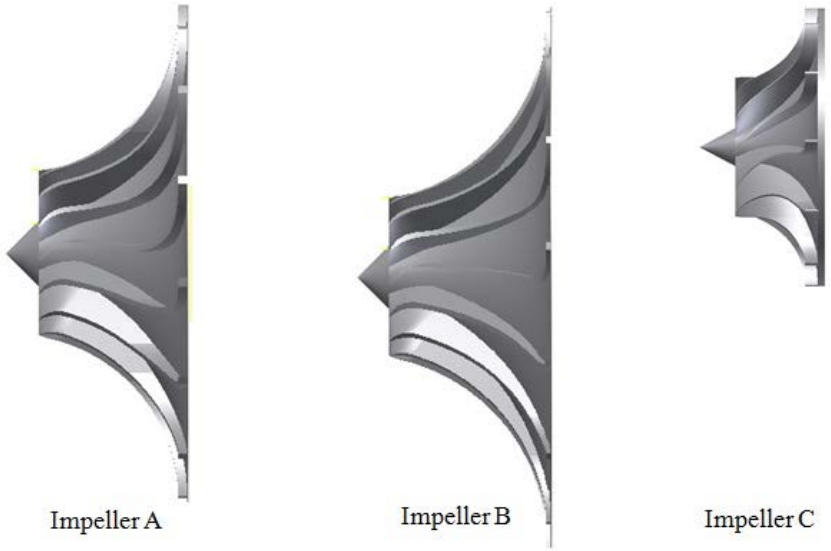


Figure 7. Different impellers tested with CFD method

Table 3. Parameters of different compressor stages used in CFD simulations

| Parameter | Unit | Compressor A | Compressor B | Compressor C |
|---|---|---|---|---|
| Speed | krpm | 47.5 | 47.5 | 75 |
| Pressure inlet | bar | 30 | 30 | 120 |
| Temperature inlet | K | 305 | 300 | 320 |
| Mass flow | Kg s-1 | 1.5 | 1.3 | 6.3 |
| Blade height | m | 0.0015 | 0.0082 | 0.0017 |
| Discharge blade angle | ° | -45 | -45 | -40 |
| Number of blades | - | 15 | 15 | 12 |
| Inlet blade angle at tip | ° | 54 | 57.6 | 61 |
| Tip clearance | m | 0.00025 | 0.00035 | 0.00025 |
| Impeller diameter | m | 0.084 | 0.094 | 0.0374 |
| Inlet hub diameter | m | 0.011 | 0.0094 | 0.005 |
| Inlet shroud diameter | m | 0.0275 | 0.027 | 0.0187 |
| Diffuser diameter | m | 0.151 | 0.188 | 0.070 |
| Axial length of impeller | m | 0.028 | 0.031 | 0.0124 |
| Shaft diameter | m | 0.025 | 0.025 | 0.014 |
| Back plate clearance | m | 0.0004 | 0.0004 | 0.0004 |

Design point operation was simulated. Each CFD model includes clearance between back plate of the impeller and the housing, so disc friction loss is included in both models (1D and numerical). Volute losses are excluded from both models.

**Numerical modeling**

Steady state CFD simulations were executed with FLUENT 13 code. The turbulence was predicted with the k-ε model and wall boundary layers were solved with logarithmic wall functions. The second-order discretization scheme was employed.

An inlet mass flow boundary condition was used with total temperature and static pressure specified (operating pressure was set to zero). Pressure outlet boundary condition with a prescribed static pressure and backflow total temperature was used for stage outlet. The turbulent kinetic energy was assumed to be uniformly distributed with intensity of 10%.

Only one blade passage was modeled and periodic boundary condition applied. Each compressor stage consisted of three volumes: impeller zone, vaneless diffuser zone and back plate clearance. Interfaces between zones adopt a frozen rotor model. This allows inlet distortion to be transferred across the different frames of reference.

Frozen rotor model can be used for turbomachinery applications in which rotor-stator interaction is relatively weak. Centrifugal compressor with vaneless diffuser and without inlet vanes can be treated as such a case [Liu and Hill (2000), Engeda et. al. (2003)]. For each compressor model mesh independence study was performed (see Table 4).

Table 4. Mesh independence study for CFD pressure and efficiency predictions

| | **Mesh size** | **$\mu_{is\ (t\text{-}t)}$** | **Average $y^+$** | **$P_{out}/P_{in\ (t\text{-}t)}$** |
|---|---|---|---|---|
| **Compressor A** | | | | |
| Grid 1 | 1.7mln | 0.806 | 290 | 1.59 |
| Grid 2 | 3.9 mln | 0.806 | 260 | 1.59 |
| Grid 3 | 8.5 mln | 0.808 | 108 | 1.59 |
| **Compressor B** | | | | |
| Grid 1 | 1.3 mln | 0.711 | 270 | 1.70 |
| Grid 2 | 3.8 mln | 0.710 | 145 | 1.70 |
| Grid 3 | 10 mln | 0.710 | 122 | 1.70 |
| **Compressor C** | | | | |
| Grid 1 | 0.9 mln | 0.908 | 614 | 1.66 |
| Grid 2 | 3.0 mln | 0.910 | 220 | 1.66 |
| Grid 3 | 7.8 mln | 0.906 | 143 | 1.67 |

Results of analytical and numerical prediction are presented in Fig 8.

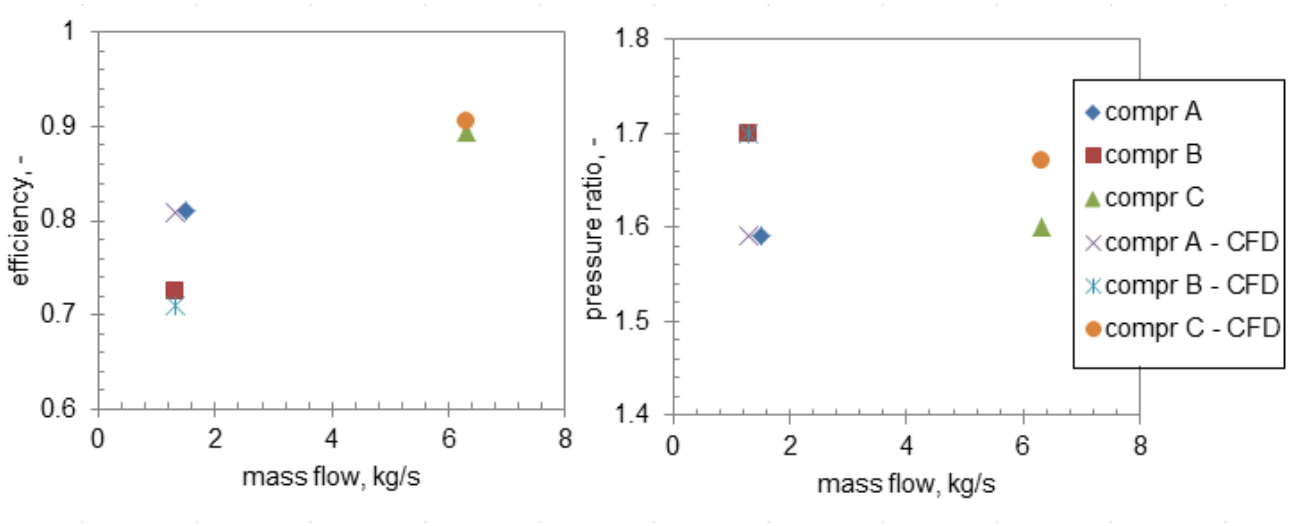


Figure 8. Comparison of analytical and numerical predictions of efficiency (t-t) and pressure ratio (t-t).

Good fit between prediction of pressure ratio and efficiency can be observed for Case A and B. For super-critical compressor (Case C) the 1D model under-predicts the pressure ratio compared to CFD. Without experimental verification it is difficult to conclude which method is more accurate in this case. It can be however expected that some general approximation present in the 1D model tend to reduce accuracy prediction in supercritical region where small under- or over-prediction of one thermodynamic property can result in significant variation of another.

An additional insight into non-dimensional performance coefficients of a machine can be beneficial in assessing efficiency predictions obtained with a given model. Most important performance coefficients for the three simulated compressors are calculated and presented in Table 5.

Table 5. Non-dimensional performance coefficients for the simulated compressors

| Parameter | Unit | Compressor A | Compressor B | Compressor C |
|---|---|---|---|---|
| Machine Mach Number | - | 0.84 | 0.95 | 0.49 |
| Flow coefficient | - | 0.021 | 0.012 | 0.064 |
| Work coefficient | - | 0.68 | 0.68 | 0.66 |
| Specific speed | - | 0.40 | 0.34 | 0.66 |
| Machine Reynolds Number | - | 7 e07 | 9 e07 | 7.1 e07 |

It can be concluded that the results of the non-dimensional analysis are quite consistent with the analytical and numerical predictions of the compressors' efficiency. The high Reynolds numbers favor reaching high efficiency in all of the presented cases. Both specific speed and flow coefficient of Compressor C are found to be within the optimal range applicable for radial compressors. It is therefore to be expected that this design will achieve the best efficiency among the tested configurations. Still, the 90% prediction of the isentropic efficiency may appear overly optimistic. If however, one takes into account relatively low pressure ratio and high molecular mass of the gas, and that the cited efficiency is calculated based on the total-to-total conditions, the prediction seems more realistic. Accordingly, a compressor with the lowest specific speed and flow coefficient and with the highest Mach numbers is expected to perform least efficiently. The lowest performance among the tested designs is predicted for Compressor B by both the analytical and numerical model.

Based on the numerical results the chart presenting the area averaged absolute Mach numbers along meridional span of the impellers is depicted in Fig 9. It is shown that for machines operating at similar pressure ratios, Reynolds numbers and work coefficients the performance is dependent on the velocity profile across the stage. Among presented cases, the compressor with the highest maximal Mach number and the steepest Mach number profile across the impeller achieves the worst efficiency.

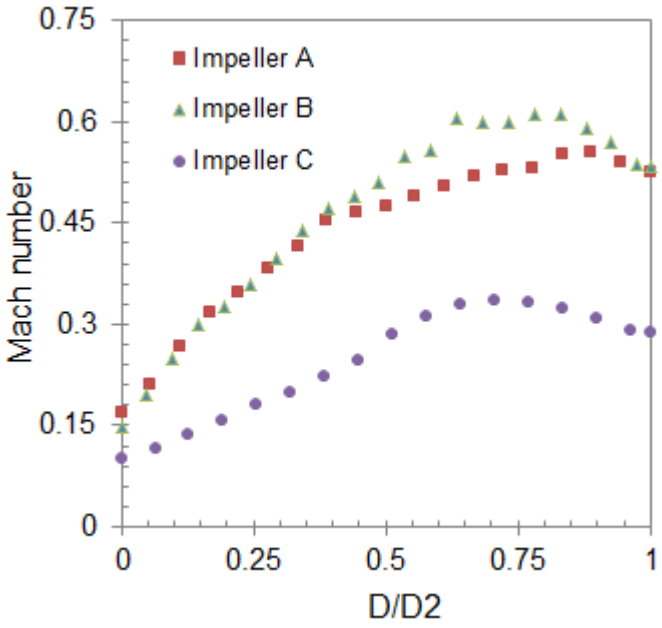


Figure.9. Numerical prediction of averaged absolute Mach numbers across the impellers

**3.2. Tool verification with existing experimental results**

SNL test results were used to validate 1D prediction of total compressor efficiency. Performance of the compressor working in its design point (no incidence at the impeller inlet) was predicted for three rotational speeds: 40, 50 and 55 krpm. In order to compare 1D prediction with experimental results the set of parameters were extracted from Sandia's report and used either as an input or a target of the simulations. For example, inlet conditions, rpms, size of the rotor were input constraints. Parameters such as impeller diameter and discharge blade height were results of the simulations obtained by adjusting other input parameters such as mass flow or absolute discharge flow angle. The list of parameters that were common for each simulation is presented in Table 6.

Table 6. Parameters of 1D simulation for Sandia's compressor

| Parameter | Unit | Value | |
|---|---|---|---|
| Pressure inlet | bar | 77 | Inputs |
| Temperature inlet | K | 305 | |
| Cavity pressure | bar | 13.8 | |
| Cavity temperature | K | 320 | |
| Number of blades | - | 12 | |
| Mean inlet blade angle | ° | 51 | |
| Tip clearance | m | 0.00025 | |
| Motor length | m | 0.168 | |
| Rotor diameter | m | 0.044 | |
| Rotor gap | m | 0.0031 | |
| Axial load | N | 1000 | |
| Axial bearing load capacity | Kg m-3 krpm-1 (lb in-3 krpm-1) | 2767 (0.1) | |
| Radial bearing load capacity | Kg m-3 krpm-1 (lb in-3 krpm-1) | 27670 (1) | |
| Seal leakage area | m2 | 1.67E-06 | |
| Dimensionless discharge coefficient | - | 2.1 | |

| | | | |
|---|---|---|---|
| Number of seal lands | - | 4 | |
| Electrical efficiency | - | 0.93 | |
| D1h/D1s | - | 0.27 | |
| B2b | ° | -50 | |
| Inlet shroud radius | m | 0.0094 | Targets |
| Inlet hub radius | m | 0.0025 | |
| Blade height | m | 0.0017 | |

Predicted efficiencies as well as the remaining results of simulations are collected in Table 7. Predicted peak compressor efficiencies agree reasonably well with experimental data where upper range of measured efficiencies (t-s) is found within 65-70% region.

Table 7. Results of the 1D simulation of Sandia's compressor

| Parameter | Unit | 45 krpm | 50 krpm | 55 krpm |
|---|---|---|---|---|
| Pressure ratio( total) | - | 1.35 | 1.43 | 1.56 |
| **Efficiency t-s** | **-** | **0.662** | **0.670** | **0.675** |
| Efficiency t-t | - | 0.698 | 0.707 | 0.714 |
| Leakage flow | % (of main mass flow) | 0.95 | 1.09 | 1.31 |
| Impeller discharge flow angle | ° | 70.3 | 71 | 73 |
| Mass flow | Kg s-1 | 2.9 | 3.1 | 3.25 |

### 3.3. Predicted loss breakdown for SNL compressor

Loss breakdown for 45 krpm machine is shown in Fig 10. Several loss mechanisms seem to have particularly pronounced impact on compressor efficiency. Small diameter of the impeller results in big relative clearance and therefore significant leakage of the gas from high to low pressure side of the blade (clearance loss). Despite significantly reduced cavity pressure high shaft speed still results in non-negligible rotor windage. Significant seal

leakage loss is a result of big pressure difference between rotor cavity and impeller back plate. This leakage is accounted in the model as a cooling. The pumping power needed to compress leaked gas from the lowered cavity pressure to the inlet pressure of the compressor is not included as it was also not included in Sandia's efficiency measurements. Electrical losses are inevitable in every kind of compressor and come from switching circuitry of the inverter and magnetic losses within the stator windings. 93% electrical efficiency was assumed according to the Sandia's report.

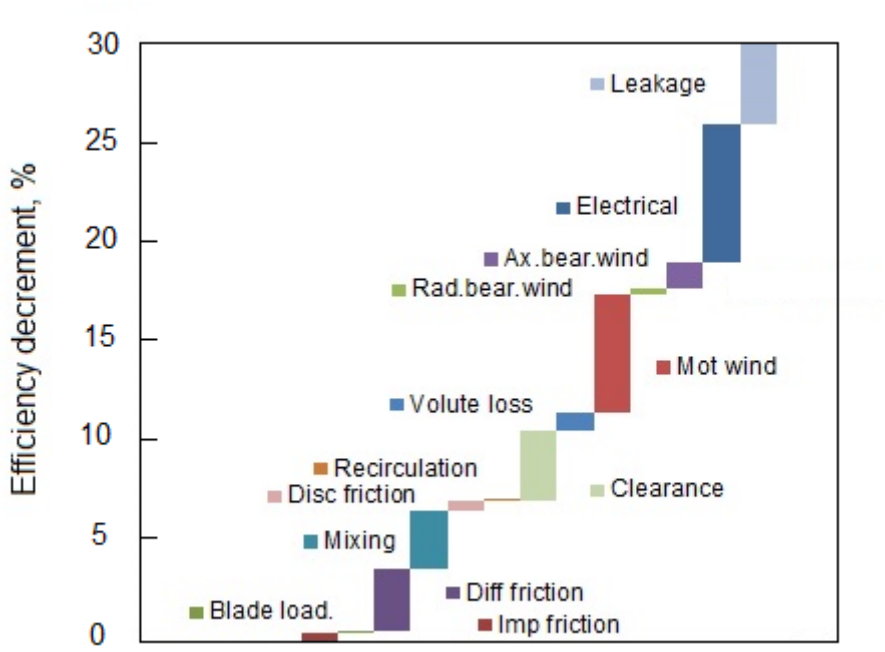


Figure 10. Loss breakdown predicted for Sandia's compressor operating at 45krpm

## 4. CONCLUSIONS

A 1D model for prediction of performance of $CO_2$ oil-free radial compressor has been proposed. 1D predictions of aerodynamic performance and pressure ratios of different compressor stages are in satisfactory agreement with results obtained with numerical methods. Efficiency predictions of a compressor model based on a 50 kW Sandia's compressor are found to correlate reasonably well with the measurements.

The $CO_2$-based turbo-machinery can be of very small sizes due to the significant density of the working fluid, especially when it is in the supercritical state. In some cases, the big relative clearance and the high surface roughness can be of a major issue when high stage efficiency is a priority. On the other hand the relatively high molecular weight of carbon

dioxide and relatively low pressure ratios present in $CO_2$ cycles favors reaching reasonably high stage efficiency of the radial compressor. It is the overall efficiency of the hermetic $CO_2$ machine that may be challenging to achieve, due to the non-stage windage and cooling losses.

Prediction of axial thrust is an important step in the $CO_2$ compressor development. Due to the complex 3-dimentional nature of the gas flow it is difficult to carry out in a quick analytical way. Various methods of thrust reduction, such as manipulations of number and diameter of impellers, adjusting the size of the labyrinth seal, varying the pressure in the motor cavity or applying pump-out vanes can be applied.

In a present form the tool requires axial thrust to be assumed. To give some preliminary orientation of a thrust magnitude that can be present in relatively small $CO_2$ compressor, a CFD method was used to analyze three different radial compressor stages with back-plate clearance. More research in the area of quick axial thrust prediction seems however very desirable.

The present model was developed with a view to assess possibility of introducing oil-free compression technology into the area of commercial grade $CO_2$ refrigeration. Hence, machines in the range of a few tens to a few hundreds of kW of shaft power are subject of interest. Rather low pressure ratios of between 2 and 3combined with at least 2 stages of compression usually result in subsonic operation; hence shock wave effects are not included in the present form of the model. The correlations predicting friction in the passages of the compressor assume smooth surfaces. Their applicability for very small geometries is therefore limited to those with a good surface finish.

.

## ACKNOWLEDGMENTS

This publication forms a part of the CREATIV project, performed under the strategic Norwegian research program RENERGI. The authors acknowledge the partners: Sintef Energy Research, Danfoss, FHL, Hydro Aluminium, John Bean Technology, Norske Skog, REMA1000, Systemair, TINE, and the Research Council of Norway (195182/S60) for their support. The authors would like to thank Barber-Nichols Inc. for the valuable comments to the present work.

## NOMENCLATURE

| | | | | | |
|---|---|---|---|---|---|
| b | blade height (m) | $\beta_{b2}$ | discharge blade angle (rad) | | |
| b* | ratio of vaneless diffuser inlet width to impeller exit width (-) | ε | clearance (m) | df | diffuser friction |
| C | absolute velocity (m s-1) | $\varepsilon_{wake}$ | wake fraction of blade-to-blade space (-) | h | hub/hydraulic |
| $c_f$ | skin friction coefficient (-) | ω | angular velocity (rad s-1) | i | Impeller channel |
| $c_M$ | Dimensionless torque coefficient (-) | W | relative velocity (m s-1) | JB | journal bearing |
| D | diameter (m) | τ | torque (N m) | LS | labirynth seal |
| $D_f$ | diffusion factor (-) | μ | viscosity (Pa s) | m | mean |
| h | specific entalphy (kJ kg-1) | ρ | density (kg m-3) | mix | mixing |
| L | length (m) | $\sigma_m$ | the motor air gap shear stress (Pa) | mot | motor's rotor |
| p | pressure (Pa) | **Subscripts** | | mw | motor windage |
| P | Power (W) | 1 | impeller inlet | r | meridional direction (angle) / meridional component |
| r | radius (m) | 2 | impeller discharge | sf | skin friction |
| Re | Reynolds number (-) | 3 | diffuser discharge | t | shroud |
| T | temperature (K) | AB | axial bearing | t-s | Total to static |
| U | impeller blade tip speed (m s-1) | bl | blade loading | t-t | Total to total |
| $Z_B$ | number of blades (-) | d | diffuser passage | θ | circumferential direction (angle) / circumferential component |
| ε | clearance (m) | cav | motor cavity | | |
| α | absolute flow angle (rad) | cl | clearance | | |

## REFERENCES

1. Bayley, F. J. and Owen, J. M., 1969. Flow Between a Rotating and Stationary Disc. Aeronautical Quarterly, Vol. 20, pp.330-354.
2. Briggs, M. H., Prahl, J. M., Bruckner R., 2008. High pressure performance of foil journal bearings in various gases, Proceedings of STLE/ASME International Joint Tribology Conference IJTC, Miami, Florida USA
3. Bruckner, R. J., 2009. Windage Power Loss in Gas Foil Bearings and the Rotor-Stator Clearance of High Speed Generators Operating in High Pressure Environments. NASA/TM—2009-215826
4. Chen, Y., Lundqvist, P., Johansson, A., Platell, P., 2006. A comparative study of the carbon dioxide transcritical power cycle compared with an organic rankine cycle with R123 as working fluid in waste heat recovery, Appl. Therm. Eng. 26, p. 2142–2147
5. Coppage, J. E., Dallenbach, F., Eichenberger, H.P., Hlavaka, G. E., Knoernschild, E. M. and Van Lee, N., 1956. Study of supersonic radial compressors for refrigeration and pressurization systems. WADC report 55-257
6. Daily, J. W. and Nece, R. E., 1960. Chamber dimension effects on induced flow and frictional resistance of enclosed rotating disks. Trans. ASME, J. Basic Eng. 82, 217–232
7. DellaCorte, C., Bruckner, R.J., 2011. Remaining Technical Challenges and Future Plans for Oil-Free Turbomachinery. J. Eng. Gas. Turb. Power., Vol. 133 / 042502-7
8. Dorfman, L. A., 1958. Hydrodynamic resistance and the heat loss of rotating solids. 1st Edition, Oliver and Boyd.
9. Dykas, B., Bruckner, R., DellaCorte, C., Edmonds, B., Prahl, J., 2009. Design, Fabrication, and Performance of Foil Gas Thrust Bearings for Microturbomachinery Applications. J. Eng. Gas. Turb. Power, Vol. 131 / 012301-7
10. Engeda, A., Kim, Y., Aungier, R., Direnzi, G., 2003. The Inlet Flow Structure of a Centrifugal Compressor Stage and Its Influence on the Compressor Performance. J Fluid Eng. Vol. 125/779
11. Hafner, A., Nekså, P., Ladam, Y., Eikevik, T.M, 2011. Oil-free R744 systems for industrial/commercial applications. ICR, Prague, Czech Republic
12. Hanselman, D., 2006. Brushless Permanent Magnet Motor Design Second Edition. Magna Physics Publishing
13. Howard, S. A., Bruckner, R. J., DellaCorte, C., Radil, K. C., 2007. Gas foil bearing technology advancements for closed Brayton cycle turbines. AIP Conf. Proc. 880, 668.
14. Japikse, D., 1982. Advanced diffusion levels in turbocharger compressors and component matching. IME conference on turbocharging and turbochargers, paper C45/82, p. 143

15. Jansen, W. A., 1967. Method for calculating the flow in a centrifugal impeller when entropy gradients are present. Royal Society Conference on Internal Aerodynamics (Turbomachinery). IME
16. Johnston, J., and Dean, R., 1966. Losses in Vaneless Diffusers of Centrifugal Compressors and Pumps. Analysis, Experiment and Design, Trans. ASME, J. Eng for Power. 88, 49–62
17. Krain, H., Hah, C., 2003. Numerical and Experimental Investigation of the Unsteady Flow Field in a Transonic Centrifugal Compressor. Proc. Int. Gas Turb. Congress, Tokyo
18. Kus, B. and Nekså, P., 2013. Oil-free turbo-compressors for CO2 refrigeration applications. Int J Refrig.
19. Liu, Z. and Hill, D. L., 2000. Issues Surrounding Multiple Frames of Reference Models for Turbo Compressor Applications. International Compressor Engineering Conference. Paper 1369.
20. Miles, A., 2011. An experimental study of windage due to rotating and static bolts in an enclosed rotor-stator system. Thermo-Fluid Mechanics Research Centre, University of Sussex.
21. Milone, D., 2011. Windage and Gas Foil Bearing Losses in a Supercritical Carbon Dioxide Turbine Generator. Supercritical CO2 Power Cycle Symposium May 24-25, 2011 Boulder, Colorado
22. Molyneaux, A., Zanelli, R., 1996. Externally Pressurized and Hybrid Bearings Lubricated with R134A for Oil-Free Compressors. International Compressor Engineering Conference at Purdue, volume II, p. 419-424
23. Natural refrigerant $CO_2$, 2009. Leonardo project "NARECO2", KHLim
24. Nekså, P., Walnum, H.T. and Hafner, A., 2010. $CO_2$ - A refrigerant from the past with prospects of being one of the main refrigerants in the future. 9th IIR Gustav Lorentzen Conference, Sydney, ISBN 978-2-913149-74-8, ISSN 0151-1637
25. Noall, J., Batton, W., 2011. Correlation of Reaction to Isentropic Velocity Ratio for a Subsonic Radial Inflow Turbine. Supercritical $CO_2$ Power Cycle Symposium, Boulder, Colorado
26. Oh, H., Yoon, E., and Chung, M., 1997. An Optimum Set of Loss Models for Performance Prediction of Centrifugal Compressors. Proc. Inst. Mech. Eng., Part A: J. of Power and Energy, Vol. 211, pp. 331–338
27. Raymond, M. S, Kasarda M. E. F., Allaire P. E., 2008. Windage Power Loss Modeling of a Smooth Rotor Supported by Homopolar Active Magnetic Bearings. J. Tribol., Vol. 130, p. 1-8
28. Roberts D. A., Steed, R., 2004. A Comparison of Steady-State Centrifugal Stage CFD Analysis to Experimental Rig Data. ANSYS/CFX Canada Int ANSYS Conf
29. Reunanen, A., Larjola, J., 2005. Radial forces in a centrifugal compressor; Experimental investigation by using magnetic bearing and static pressure distribution. J. Therm. Sci., Vol. 14, No.1., p 1-8

30. Schiffmann, J., Favrat, D., 2009. Experimental investigation of a direct driven radial compressor for domestic heat pumps. Int. J. Refrig. 32, 1918 – 1928
31. Schiffmann, J., Favrat, D., 2010. Design, experimental investigation and multi-objective optimization of a small-scale radial compressor for heat pump applications. Energy. 35/8, 436-450
32. Schlichting, H., 1968. Boundary-Layer Theory. McGraw-Hill, New York
33. Shi, W., Wang, H., Zhou, L., Zou, P., Wang, C., 2010. The estimation and experiment of axial force in deep well pump basing on numerical simulation. . IJMECS Vol.2, 53-61
34. Sukhomlinov, I. Ya., Golovin, M. V., Tagantsev, O. M., Ravikovich, Yu. A., Ermilov, Yu. I., Kholobtsev, D. P., 2003. Power Loss In a Built-in High-Frequency Electric Drive For a Centrifugal Refrigeration Compressor. Chem. Petrol. Eng., Vol. 39, Nos. 7–8
35. Sungho, Y., Baek, J. H., 2001. A sensitivity analysis of centrifugal compressors' empirical models. KSME Int. J., Vol. 15 No.9, pp. 1291-1201
36. Swain, E., 2005. Improving a one-dimensional centrifugal compressor performance prediction method. Proc.Inst.Mech.Eng., Part A: J. of Pow. and Ene. 2005 219: 653
37. von Kármán, T., 1921. Technical Memorandum on Laminar and Turbulent Friction. National advisory committee for aeronautics, Report No. 1092.
38. Vrancik, J. E., 1968. Prediction of windage power loss in alternators. NASA Technical Note D-4849.
39. Walton, J. F., Heshat, H., Tomaszewski, M., 2012. Power loss in high-speed micro-machinery – an experimental study. Proc. of ASME Turbo Expo
40. Whitfield, A., Baines, N.C., 1990. Design of radial turbomachines. Longman Scientific & Technical
41. Wright, S.A., Radel, R.F., Vernon, M.E., Rochau, G.E., Pickard, P.S., 2010. Operation and Analysis of a Supercritical $CO_2$ Brayton Cycle, Sandia Report SAND2010-0171
42. Xu, C., Amano, R. S., 2009. Development of a Low Flow Coefficient Single Stage Centrifugal Compressor. Int. J. Comput. Methods Eng. Sci Mech.., 10:282–289
43. Zhang, X.R., Yamaguchi, H., Uneno, D., Fujima, K., Enomoto, M., Sawada, N., 2006. Analysis of a novel solar energy-powered Rankine cycle for combined power and heat generation using supercritical carbon dioxide, Renew. Energ., 31, p. 1839–1854